Strain-Tunable Interlayer Magnetic Coupling in van der Waals Ferromagnet Fe_3GaTe_2 Nanoflakes

Sinan Liu(刘思男)[1,2], Chuandi Pan(潘传迪)[1,2], Chunsheng Wang(王春生)[1,2], Hengning Wang(王恒宁)[1,2], Dongna Feng(冯东娜)[3], Gaojie Zhang(张高节)[4,5], Hao Wu(武浩)[4,5], Haixin Chang(常海欣)[4,5,6], Huanhuan Zhang(张欢欢)[7], Jin Tang(汤进)[7*], Qilong Sun(孙启龙)[3*], Guolin Zheng(郑国林)[1*], and Mingliang Tian(田明亮)[1]

[1]*Anhui Provincial Key Laboratory of Low-Energy Quantum Materials and Devices, High Magnetic Field Laboratory, HFIPS, Chinese Academy of Sciences, Hefei 230031, China*
[2]*University of Science and Technology of China, Hefei 230026, China*
[3]*School of Science, Shandong Jianzhu University, Jinan 250100, China*
[4]*Center for Joining and Electronic Packaging, State Key Laboratory of Material Processing and Die & Mold Technology, School of Materials Science and Engineering, Huazhong University of Science and Technology, Wuhan 430074, China*
[5]*Wuhan National High Magnetic Field Center and Institute for Quantum Science and Engineering, Huazhong University of Science and Technology, Wuhan 430074, China*
[6]*Shenzhen R&D Center of Huazhong University of Science and Technology (HUST), Shenzhen 518000, China*
[7]*State Key Laboratory of Opto-Electronic Information Acquisition and Protection Technology, School of Physics, Anhui University, Hefei 230601, China*

(Received 8 December 2025; accepted manuscript online 10 March 2026)

Interlayer magnetic coupling plays vital roles in the physical properties of van der Waals (vdW) magnets and in engineering functionally optimized spintronics. So far, however, few avenues are available to control the magnetic coupling at interfaces. Here, we report that the interlayer ferromagnetic–antiferromagnetic coupling in Fe_3GaTe_2, an above-room-temperature vdW ferromagnet, can be largely enhanced by in-plane tensile strain implemented via a flexible substrate, leading to a large zero-field-cooled exchange bias (EB) with a maximal EB field H_{EB} up to 1.7 kOe at 50 K. A positive correlation between the EB field H_{EB} and coercivity H_c is further revealed in strained Fe_3GaTe_2 nanoflakes. Theoretical analysis combining micromagnetic simulation and density functional theory (DFT) reveals that strain enhances interlayer exchange coupling, giving rise to EB effects. A nonmonotonic evolution of coercivity with respect to tensile strain along a general crystallographic direction within the *ab*-plane is further demonstrated by DFT calculations, aligning qualitatively with experimental findings. Our work provides an alternative knob to tune interlayer coupling in vdW materials, enabling tailoring of magnetism and other correlated states at interfaces.

DOI: 10.1088/0256-307X/43/4/040710 CSTR: 32039.14.0256-307X.43.4.040710

Two-dimensional (2D) van der Waals (vdW) magnets[1–3] have drawn extensive attention due to their unique tunability at the nanometer scale and have played crucial roles in spintronics and modern information technology. The interlayer magnetic coupling, although very weak due to the large vdW gap, usually determines the magnetic properties—such as the magnetic ground state and easy axis—in vdW magnets. To date, few avenues can be utilized to control the interlayer magnetic coupling, such as pressure,[4,5] protonic gating,[6,7] and laser shocking.[8] Tensile strain has recently proved to be an effective way to tune magnetism[9,10] as well as excitonic behaviors[11–13] in vdW semiconducting heterostructures. However, it is still unclear whether the interlayer magnetic coupling in vdW magnets can be experimentally modulated by in-plane tensile strain.

In this work, we investigate the magnetic transport properties of vdW magnet Fe_3GaTe_2 (FGaT) nanoflakes by applying an in-plane tensile strain via flexible substrates. A large zero-field-cooled (ZFC) exchange bias (EB) with a maximal EB field H_{EB} up to 1.7 kOe at 50 K emerges in strained FGaT nanoflakes. Further study reveals a positive correlation between the EB field H_{EB} and the coercivity H_c in strain-tuned FGaT nanoflakes, leading to an anomalous peak of the EB field near 50 K with a tensile strain of $\varepsilon = 0.28\%$. Theoretical analysis based on micromagnetic simulation and density functional theory (DFT) calculations reveals a strain-enhanced interlayer exchange coupling and resultant EB effects. Supported by DFT calculations, both magnetic coupling and

*Corresponding authors. Email: jintang@ahu.edu.cn; long.q.sun@gmail.com; glzheng@hmfl.ac.cn
© 2026 Chinese Physical Society and IOP Publishing Ltd. All rights, including for text and data mining, AI training, and similar technologies, are reserved.

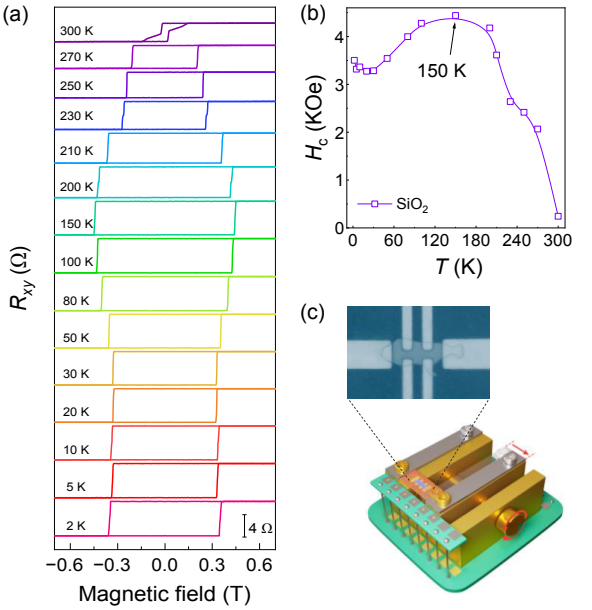

Fig. 1. (a) Magnetic hysteresis loops at various temperatures for the Fe_3GaTe_2 device #1 on a SiO_2/Si substrate. (b) Temperature dependence of H_c from 2 K to 300 K. (c) Schematic of the strain apparatus for tensile strain application and a zoomed-in view of the optical micrograph of device #2 on a PI substrate.

magnetic anisotropy energy (MAE) are found to be dramatically tuned by in-plane tensile strain along a general crystallographic direction within the *ab*-plane, consistent with the observed nonmonotonic evolutions of both the EB field and coercivity with respect to the tensile strain in experiments. Our findings demonstrate that in-plane tensile strain can effectively tune interlayer magnetic coupling, offering a mechanism for strain-engineered spintronics.

FGaT is a recently discovered above-room-temperature vdW magnet[14] that has been extensively investigated. Its crystal exhibits a hexagonal structure with space group $P6_3/mmc$ ($a = b = 3.9860$ Å, $c = 16.2290$ Å, $\alpha = \beta = 90°$, $\gamma = 120°$), and it is a ferromagnet with a Curie temperature (T_c) of ∼350–380 K and large perpendicular magnetic anisotropy (PMA).[14] Figure 1(a) shows square-shaped magnetic hysteresis loops at various temperatures ranging from 2 K to 300 K in a FGaT flake on a SiO_2/Si substrate under out-of-plane magnetic fields, consistent with the large PMA in FGaT. The coercivity generally decreases as the temperature increases, as in FGaT[15] and Fe_5GeTe_2,[16] due to thermal fluctuations. However, an anomalous temperature dependence of coercivity is shown in Fig. 1(b), akin to observations reported previously:[17] that is, coercivity increases from 30 K to 150 K, followed by a sharp decrease at higher temperatures. The underlying mechanism has so far remained unclear, possibly due to intricate magnetic phases.[18] To apply an in-plane tensile strain onto FGaT, we first exfoliate FGaT flakes onto SiO_2/Si substrates, then transfer the selected flakes onto flexible polyimide (PI) substrates using a dry transfer technique, similar to the method used in previous work.[9] Subsequently, standard ultraviolet lithography is used to fabricate Hall bar devices, followed by electrical contact deposition via magnetron sputtering. The device is finally screwed onto a strain apparatus, as depicted schematically in Fig. 1(c), where the device can be elongated by rotating the right knob clockwise. The optical image of device #2 is also presented above the strain cell, as shown in Fig. 1(c). To estimate the applied tensile strain on FGaT, the strain is defined as $\varepsilon = \Delta L/L$, where L represents the length of the unstrained sample and ΔL is its change in length under strain. Before the measurements, all devices were spin-coated with PMMA to prevent contamination.

To investigate the influence of tensile strain on the magnetic properties of FGaT flakes, the magnetic hysteresis loops are measured under different tensile strains at 2 K, as shown in Fig. 2(a). Notably, a ZFC EB effect emerges at 0.11% strain, yielding an EB field of $H_{EB} = 767$ Oe compared to the unstrained situation ($H_{EB} = 0$ Oe), probably due to the strain-induced enhancement of ferromagnetic (FM)–antiferromagnetic (AFM) exchange coupling. Increasing the strain, the EB field remains positive before transitioning to a negative value at a strain of 0.33%. This crossover from a positive to a negative EB effect is probably due to the change in exchange coupling at the FM–AFM interface from FMI-1 (↑/↓↑) to FMI-2 (↓/↓↑), analogous to that in previous work.[19] The EB effect then disappears with further strain increase and re-emerges at 1.15%. We hypothesize that the energy of the AFM coupling is approximately equal to that of the FM coupling at the interface. This may cause FM and AFM couplings to alternate, even within a single hysteresis loop, so that the EB effect can be positive, negative, or zero, akin to the previous study.[6] Remarkably, the EB effect undergoes a similar but more dramatic evolution at 50 K, as shown in Fig. 2(b). As the strain increases to 0.28%, for example, the EB field reaches a maximum of 1708 Oe, compared to 607 Oe at 2 K. Figure 2(b) further shows that the amplitude of the negative EB effect at 50 K is more than three times larger than that at 2 K under the same tensile strain of 0.33%. Generally, H_{EB} decreases as the temperature increases. This anomalous H_{EB} peak near 50 K will be discussed later. Similar fluctuations of EB fields with tensile strain have also been observed in device #4, as shown in Supplementary Materials (SM) Fig S1. Based on the experimentally measured magnetic parameters of FGaT,[14] we performed micromagnetic simulations to investigate the EB effect. According to the previous study, AFM layers may arise from doping.[19] In our simulation, a few AFM layers were randomly intercalated within the FM FGaT matrix, as illustrated in the inset of Fig. 2(c). Our simulations show that the non-zero interlayer exchange coupling A between these FM and AFM layers gives rise to an EB effect in the FM region and that the amplitude of the EB field is proportional to the strength of this interlayer coupling, as illustrated in Fig. 2(c) and SM Fig. S2. Notably, when the interlayer exchange coupling switches from an AFM type to a FM type, the EB field reverses its sign. These results suggest that the experimentally observed strain-tunable EB effects originate from strain-modulated interlayer exchange coupling, as will be discussed later.

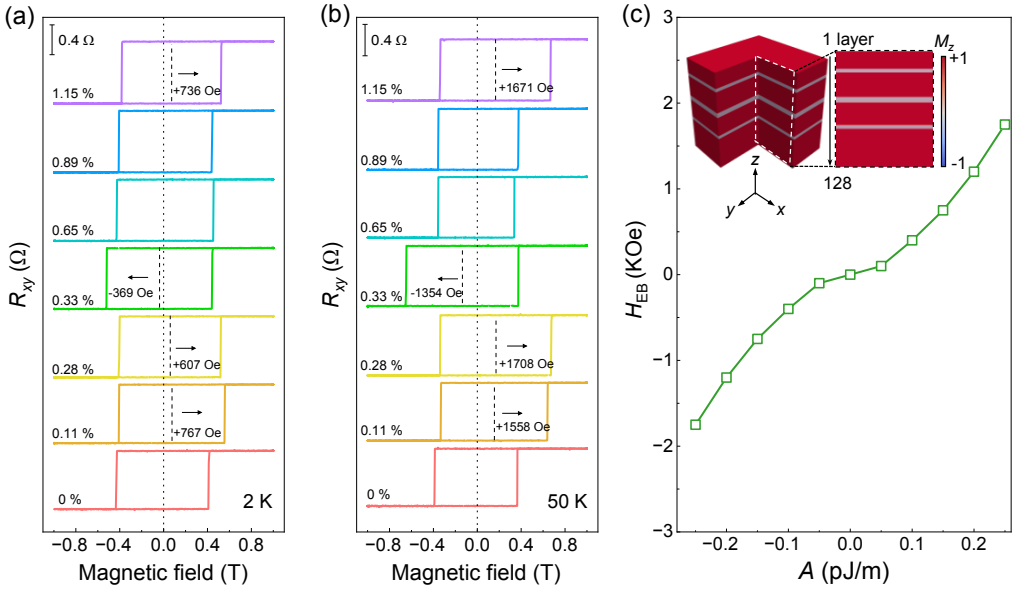

Fig. 2. Magnetic hysteresis loops under different strains for (a) 2 K and (b) 50 K in device #2. Both positive and negative EB effects are observed under in-plane tensile strain. The maximal EB field H_{EB} reaches 1708 Oe at $T = 50$ K with $\varepsilon = 0.28\%$. (c) Exchange coupling coefficient A dependence of the EB field H_{EB}. Inset: micromagnetic simulation model. The color represents the out-of-plane magnetization according to the color bar.

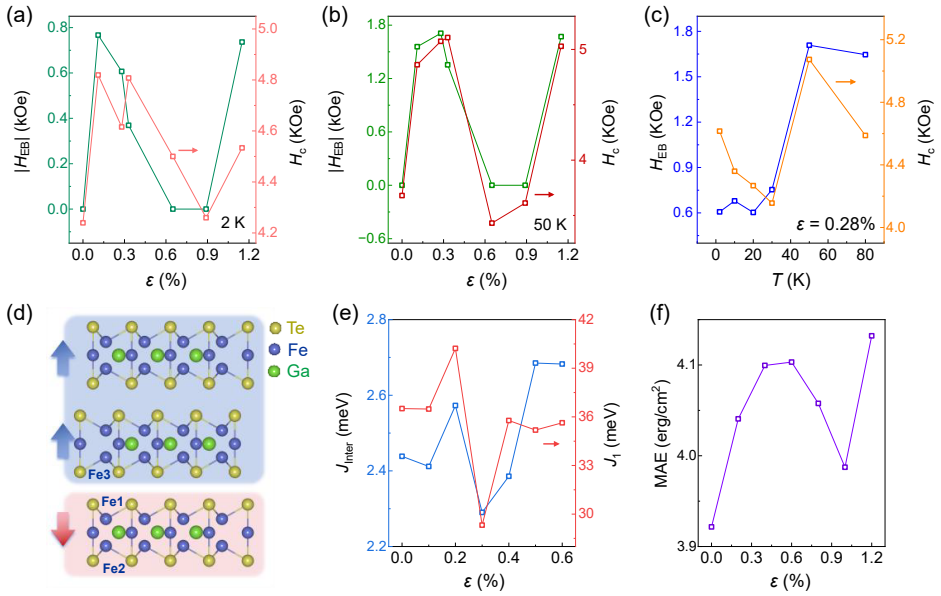

Fig. 3. Evolution of $|H_{EB}|$ (left axis) and H_c (right axis) as a function of strain at (a) 2 K and (b) 50 K in device #2. (c) Evolution of H_{EB} (left axis) and H_c (right axis) as a function of temperature at 0.28% strain. (d) Illustration of the structural and magnetic configurations of a FGaT model. The blue spheres represent Fe atoms. (e) Evolution of J_{Inter} (left axis) and J_1 (right axis) as a function of strain. (f) Evolution of MAE as a function of strain, obtained from DFT calculations.

Figures 3(a) and 3(b) present the strain dependence of $|H_{EB}|$ and H_c at two different temperatures, where $|H_{EB}| = |H_c^+ + H_c^-|/2$ and $H_c = (H_c^+ - H_c^-)/2$, with H_c^+ and H_c^- representing the positive and negative coercive fields as the magnetization reaches zero, respectively. The data show that $|H_{EB}|$ exhibits a nonmonotonic evolution with respect to strain, and a similar behavior in H_c is also observed. We note a strikingly positive correlation between $|H_{EB}|$ and H_c at both 2 K and 50 K, except at $\varepsilon = 0.33\%$, where the EB effect switches from positive to negative. As discussed previously,[20] the change in coercivity is attributed to the variation in pinning of the Fe domain walls, which is positively associated with the exchange coupling responsible for EB effects at interfaces. A similar mechanism might also exist in FGaT. We note, however, that the crossover from positive to negative EB effects, as the strain varies from 0.28% to 0.33%, is always accompanied by an enhancement in coercivity. This is possibly due to magnetic frustration at the FM–AFM interface induced by strain.[18,20] Figure 3(c) further illustrates the temperature dependence of H_{EB} and H_c at $\varepsilon = 0.28\%$. We observe a clear maximum in H_{EB} at about

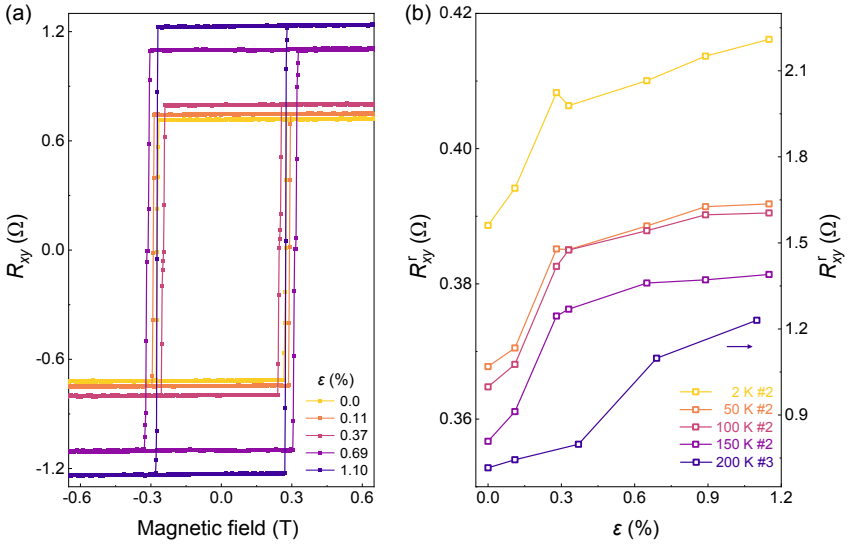

Fig. 4. (a) Evolution of magnetic hysteresis loops with respect to strain at 200 K for device #3. (b) Evolution of $R^{\rm r}_{xy}$ as a function of strain for device #2 at four selected temperatures from 2 K to 150 K and for device #3 at 200 K.

50 K. Generally, $H_{\rm EB}$ decreases with increasing temperature. However, the coercivity $H_{\rm c}$ increases with temperature from 30 K to 150 K, as shown in Fig. 1(b). Thus, the positive correlation between $H_{\rm c}$ and $H_{\rm EB}$ leads to a maximum in the EB field at 50 K.

To elucidate the underlying mechanism of the anomalous evolution of the EB effect with respect to in-plane tensile strain, we performed DFT calculations on a trilayer FGaT model. The magnetic coupling state was constructed to mimic the experimental FM–AFM interface, with the top two layers ferromagnetically aligned and the bottom layer coupled antiferromagnetically to the upper block, as illustrated in Fig. 3(d). In Fig. 3(e), the calculated interlayer exchange coupling strength ($J_{\rm Inter}$ between Fe1 and Fe3) exhibits a nonmonotonic evolution with respect to the in-plane tensile strain. As illustrated by the micromagnetic simulation above, the magnitude of the EB field is intrinsically proportional to the interfacial coupling energy ($H_{\rm EB} \propto J_{\rm Inter}$), leading to a similar strain dependence of the EB field in Figs. 3(a) and 3(b). We attribute this behavior to the sensitivity of the Fe–Fe orbital hybridization and superexchange paths across the vdW gap. The tensile strain alters the bond angles and interlayer distances, thereby modulating the competition between the FM and AFM superexchange interactions. Moreover, the calculated intralayer coupling (J_1 between Fe1 and Fe2) follows a similar trend, which correlates well with the strain-dependent coercivity $H_{\rm c}$, as $H_{\rm c}$ is governed by the intrinsic MAE and exchange stiffness. Figure 3(f) illustrates the calculated MAE of the FM–AFM interface under varying strains along a general crystallographic direction within the *ab*-plane. As can be seen, the strain-dependent MAE curve qualitatively reproduces the $H_{\rm c}$ behavior observed in Figs. 3(a) and 3(b). Note that the tensile strain modifies the lattice parameters, thereby influencing the spin–orbit coupling and the electronic band structure near the Fermi level. This structural modification results in the fluctuation of the MAE shown in Fig. 3(f).

We then examined the effects of tensile strain on the remanent Hall resistance by performing Hall measurements. Figure 4(a) shows the Hall resistance as a function of the applied magnetic field under different strains (from 0% to 1.10%) at 200 K in device #3. We find that the remanent Hall resistance can be dramatically tuned by strain. Figure 4(b) plots the strain-dependent remanent Hall resistance with the strain varying from 0% to 1.15% at several selected temperatures, where $R^{\rm r}_{xy}$ is determined by $R^{\rm r}_{xy} = (R^{+}_{xy} - R^{-}_{xy})/2$, with R^{+}_{xy} and R^{-}_{xy} representing the positive and negative remanent Hall resistances as the magnetic field approaches zero, respectively. In addition, the remanent Hall resistance $R^{\rm r}_{xy}$ is proportional to the spontaneous magnetization M_z that contributes to the anomalous Hall effect, according to $R_{xy} = R_0 H_z + R_{\rm s} M_z$, where $R_{xy} = R^{\rm r}_{xy}$ at $H_z = 0$. Therefore, the significant increase in $R^{\rm r}_{xy}$ clearly demonstrates the enhancement of the anomalous Hall effect achieved through strain, similar to the increase in anomalous Hall resistance observed previously under pressure.[21] The enhancement of anomalous Hall resistance under in-plane tensile strain is further confirmed in device #4 and is also qualitatively consistent with theoretical calculations, as shown in SM Fig. S3.

In conclusion, we experimentally demonstrate that EB, coercivity, and anomalous Hall resistance can be modulated by in-plane uniaxial tensile strain through flexible PI substrates in the ferromagnet FGaT. A positive correlation between the EB field and coercivity is revealed. Combining micromagnetic simulations and DFT calculations, we find that tensile strain can dramatically tune magnetic exchange coupling and MAE along a general crystallographic direction within the *ab*-plane, giving rise to nonmonotonic evolutions of both the EB effect and coercivity with respect to strain. Our findings demonstrate that in-plane tensile strain is an effective means of tuning interlayer magnetic coupling in FGaT, enabling the tailoring of interface coupling in other vdW heterointerfaces.

Methods. Transport measurements were performed using a commercial Physical Property Measurement System (CryoM-9-PT, Physike Technology) with magnetic field up to 9 T.

Zero-temperature micromagnetic simulations of EB effects in ∼100 nm-thick lamellae were performed using MuMax3.[22] The Hamiltonian included the exchange interaction energy (A), uniaxial MAE (K_u), Zeeman energy, and dipole–dipole interaction energy. The simulation parameters were based on FGaT, with a PMA constant $K_u = 388\,\mathrm{kJ\cdot m^{-3}}$, a saturation magnetization $M_s = 438.5\,\mathrm{kA\cdot m^{-1}}$, and an exchange constant $A = 10\,\mathrm{pJ\cdot m^{-1}}$ for the FM layers and $A = -10\,\mathrm{pJ\cdot m^{-1}}$ for the AFM layers. The computational cell size was set to $5\times5\times0.81\,\mathrm{nm^3}$, with a total of $20\times20\times125$ cells, under 2D periodic boundary conditions. Layers 21–23, 51–55, and 80–82 were defined as AFM phases, while the remaining layers were treated as FM [Fig. 2(c)]. The interlayer exchange coupling was varied to examine its influence on the EB. It should be noted that while the magnitude of the EB can be influenced by the number and distribution of AFM layers, the overall trend remains consistent with experimental observations.

First-principles DFT calculations were performed utilizing the plane-wave pseudopotential method based on the Perdew–Burke–Ernzerhof exchange-correlation functional, as implemented within the Quantum ESPRESSO package.[23,24] For the trilayer FGaT structure with the FM–AFM interface, the atomic positions were fully relaxed until all residual forces on each atom were smaller than 10^{-4} eV/Å, and the energy convergence criterion was set to 10^{-7} eV. The plane-wave cutoff energy was 70 Ry, and a $10\times18\times1$ Monkhorst-pack grid in the Brillouin zone was used in the self-consistent calculations. The DFT-D3 method of Grimme was used to treat the vdW interaction for the FM–AFM interface in FGaT.[25] To properly describe the FGaT system, a vacuum spacing of 20 Å was introduced along the z direction to avoid spurious interactions between periodic images.

Acknowledgements. This work was supported by the National Key R&D Program of the MOST of China (Grant Nos. 2024YFA1611103 and 2022YFE0134600), the National Natural Science Foundation of China (Grant Nos. 12274413, 52272152, 12422403, and U24A6001), the Basic Research Program of the Chinese Academy of Sciences (CAS) Based on Major Scientific Infrastructures (Grant No. JZHKYPT-2021-08), the Anhui Provincial Major S&T Project (Grant No. s202305a12020005), the High Magnetic Field Laboratory of Anhui Province (Grant No. AHHM-FX-2020-02), the Collaborative Innovation Program of Hefei Science Center, CAS (Grant No. 2022HSC-CIP017), the Shenzhen Science and Technology Innovation Committee (Grant No. JCYJ20230807143614031), and the Scientific Research Innovation Capability Support Project for Young Faculty (Grant No. SRICSPYF-BS2025073).

References

[1] Gong C, Li L, Li Z, Ji H, Stern A, Xia Y, Cao T, Bao W, Wang C, Wang Y, Qiu Z Q, Cava R J, Louie S G, Xia J, and Zhang X 2017 *Nature* **546** 265

[2] Huang B, Clark G, Navarro-Moratalla E, Klein D R, Cheng R, Seyler K L, Zhong D, Schmidgall E, McGuire M A, Cobden D H, Yao W, Xiao D, Jarillo-Herrero P, and Xu X 2017 *Nature* **546** 270

[3] Deng Y, Yu Y, Song Y, Zhang J, Wang N Z, Sun Z, Yi Y, Wu Y Z, Wu S, Zhu J, Wang J, Chen X H, and Zhang Y 2018 *Nature* **563** 94

[4] Song T, Fei Z, Yankowitz M, Lin Z, Jiang Q, Hwangbo K, Zhang Q, Sun B, Taniguchi T, Watanabe K, McGuire M A, Graf D, Cao T, Chu J H, Cobden D H, Dean C R, Xiao D, and Xu X 2019 *Nat. Mater.* **18** 1298

[5] Li T, Jiang S, Sivadas N, Wang Z, Xu Y, Weber D, Goldberger J E, Watanabe K, Taniguchi T, Fennie C J, Fai Mak K, and Shan J 2019 *Nat. Mater.* **18** 1303

[6] Zheng G, Xie W Q, Albarakati S, Algarni M, Tan C, Wang Y, Peng J, Partridge J, Farrar L, Yi J, Xiong Y, Tian M, Zhao Y J, and Wang L 2020 *Phys. Rev. Lett.* **125** 047202

[7] Albarakati S, Xie W Q, Tan C, Zheng G, Algarni M, Li J, Partridge J, Spencer M J S, Farrar L, Xiong Y, Tian M, Wang X, Zhao Y J, and Wang L 2022 *Nano Let.* **22** 6166

[8] Huang X, Zhang L, Tong L, Li Z, Peng Z, Lin R, Shi W, Xue K H, Dai H, Cheng H, de Camargo Branco D, Xu J, Han J, Cheng G J, Miao X, and Ye L 2023 *Nat. Commun.* **14** 2190

[9] Wang Y, Wang C, Liang S J, Ma Z, Xu K, Liu X, Zhang L, Admasu A S, Cheong S W, Wang L, Chen M, Liu Z, Cheng B, Ji W, and Miao F 2020 *Adv. Mater.* **32** 2004533

[10] Cenker J, Sivakumar S, Xie K, Miller A, Thijssen P, Liu Z, Dismukes A, Fonseca J, Anderson E, Zhu X, Roy X, Xiao D, Chu J H, Cao T, and Xu X 2022 *Nat. Nanotechnol.* **17** 256

[11] Conley H J, Wang B, Ziegler J I, Haglund R F, Pantelides S T, and Bolotin K I 2013 *Nano Lett.* **13** 3626

[12] Desai S B, Seol G, Kang J S, Fang H, Battaglia C, Kapadia R, Ager J W, Guo J, and Javey A 2014 *Nano Lett.* **14** 4592

[13] Pak S, Lee J, Lee Y W, Jang A R, Ahn S, Ma K Y, Cho Y, Hong J, Lee S, Jeong H Y, Im H, Shin H S, Morris S M, Cha S, Sohn J I, and Kim J M 2017 *Nano Lett.* **17** 5634

[14] Zhang G, Guo F, Wu H, Wen X, Yang L, Jin W, Zhang W, and Chang H 2022 *Nat. Commun.* **13** 5067

[15] Fei Z, Huang B, Malinowski P, Wang W, Song T, Sanchez J, Yao W, Xiao D, Zhu X, May A F, Wu W, Cobden D H, Chu J H, and Xu X 2018 *Nat. Mater.* **17** 778

[16] May A F, Ovchinnikov D, Zheng Q, Hermann R, Calder S, Huang B, Fei Z, Liu Y, Xu X, and McGuire M A 2019 *ACS Nano* **13** 4436

[17] Chen X, Luo Q Y, Guo P J, Zhou H J, Hu Q C, Wu H P, Shen X W, Cui R Y, Dong L, Wei T X, Xiao Y H, Li D, Lei L, Zhang X, Wang J F, and Xiang G 2024 *Adv. Funct. Mater.* **35** 2413529

[18] Lee S E, Li Y, Lee Y, Brown W K, Cai P, Yun J, Lee C, Moon A, Mei L, Kim J, Xin Y, Borchers J A, Heitmann T W, Frontzek M, Ratcliff W D, McCandless G T, Chan J Y, Santos E J G, Kim J, Phatak C M, Kulichenko V, and Balicas L 2025 *ACS Nano* **19** 28702

[19] Wang C, Wang J, Xie W Q, Zhang G, Wu H, Zhou J, Zhu X, Ning W, Wang G, Tan C, Wang L, Du H, Zhao Y J, Chang H, Zheng G, Geng W T, and Tian M 2023 *Phys. Rev. B* **107** L140409

[20] Leighton C, Nogués J, Jönsson-Åkerman B J, and Schuller I K 2000 *Phys. Rev. Lett.* **84** 3466

[21] Iimori R, Hu S, Mitsuda A, and Kimura T 2024 *Commun. Mater.* **5** 235

[22] Vansteenkiste A, Leliaert J, Dvornik M, Helsen M, Garcia-Sanchez F, and Van Waeyenberge B 2014 *AIP Advances* **4** 107133

[23] Giannozzi P, Baroni S, Bonini N *et al.* 2009 *J. Phys.: Condens. Matter* **21** 395502

[24] Perdew J P, Burke K, and Ernzerhof M 1996 *Phys. Rev. Lett.* **77** 3865

[25] Grimme S, Antony J, Ehrlich S, and Krieg H 2010 *J. Chem. Phys.* **132** 154104